ORIGINAL PAPER

Investigations on electronic and optical properties of Zn:CdO-PVDF polymer composite thin films

M. Yousaf[1] · **M. Junaid Iqbal Khan**[1] · **Zarfishan Kanwal**[1] · **Shahid M. Ramay**[2] · **Hamid Shaikh**[3] · **Murtaza Saleem**[4]

Abstract

Polymer-based nanocomposites are considered to be next generation key materials for the modern electronic and photo energy devices. In the current research, computational and experimental investigations on Zn incorporated CdO-PVDF polymer composite thin films were carried out. After achieving a good optical response of Zn substituted CdO at various Zn concentrations using the Wien2k code, pure and Zn-doped CdO nanorods were prepared using the co-precipitation method. Afterward, uniform thin films of Zn:CdO-PVDF polymer composites were deposited. SEM analysis reveals fiber like morphology of PVDF and rod-like morphology is noticed after adding Zn contents in CdO-PVDF matrix. These morphological changes lead us to tune the optical response of the selected polymer composites. Elemental composition analysis confirmed the presence of expected elements in dissolved amounts in each composition. An enhanced absorption trend of the polymer composites in the visible region is observed which points their potential uses in fabrication of visible modern optoelectronic devices.

Extended author information available on the last page of the article

Graphical abstract
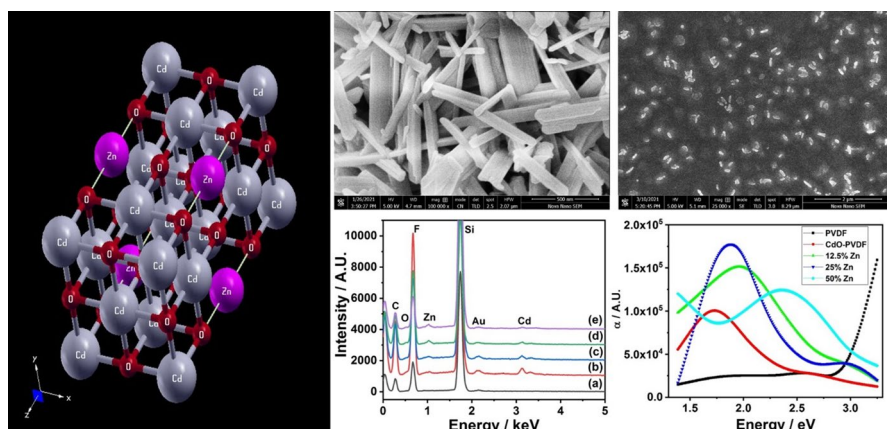
Keywords PVDF nanocomposites · Cadmium oxide · Ab-initio calculations · Optical properties

Introduction

Research on polymers has triggered the advancements in material science and these materials may commercially be used for the production of flexible electronic devices. The novelty of the polymer based materials emerges owing to their capacity and utility to fabricate inexpensive, portable, reliable, high output and rapid devices [1]. Their rapid progression in the fields of biomedical [2], microelectronic [3], opto-electronics [4], and spintronics [5] involves polymer materials which lead to many important discoveries in material science. The development of the polymer based materials has been tremendously increased due to their biodegradability and green energy applications. However, low cost, excellent mechanical strength, and environment friendliness of polymers emphasize their uses in the recent microelectronic and semiconducting devices. Recently, polymer based materials have come forward owing to their commercial and industrial applications as their properties may be dramatically improved by varying the concentrations or by adding other materials into the host polymer matrix. In order to modulate the properties of polymers as required for the desired performance in various fields, the polymers are mixed with other materials to form the composites. Hence, polymer matrix based composites has been an efficient and influential method for tuning the properties of polymers [6, 7]. In current era, the modern technology based on the electronic devices requires the investigation of materials with high dielectric constant having low dielectric loss and have enhanced dielectric strength [8, 9].

Polymers have been used as a matrix with the nanoparticle fillers in order to prepare composite materials which possess exceptional optical, electronic, dielectric

and mechanical properties [10–12]. Due to the outstanding properties of polymer composite materials, they have wide applications in the field of biomedical sensing [13], solar cells [14], electrochemical actuators [15], artificial muscles [16], and next generation of capacitors for energy storage applications [17]. These polymer composite materials fulfill the needs of the industry due to their improved mechanical strength, suitable dielectric properties, easy fabrication, exciton binding energy, noble power conversion efficiency with higher rate of charge recombination, and low cost economy.

Polyvinylidene difluoride (PVDF) is synthetic polymer which is water soluble and is used as host material for different nanoparticles. It has biocompatibility, good mechanical properties, chemical stability, and optical clarity [18]. It is studied considerably and preferred in research due to high abrasion, tensile strength, good charge storage capacity, elongation, easy processability, low manufacturing cost along with the thermal and chemical stability [19–21]. The PVDF is tailored by incorporating some filler onto its matrix in order to channelize toward specific applications. So, a wide scope always exists in exploring the properties of polymer nano composite while using PVDF as host polymer matrix. Researchers have demonstrated that the nanoparticles of metal oxide in the polymer matrix have surprisingly enhanced the negative charge carriers and shows robust interactions with the positive charge carriers of the polymer surface [22–29]. Hence, transition metal oxides are taken as outstanding candidate for the energy storage capacity due to good dispensability in the polymer matrix [30, 31]. Cadmium oxide (CdO) is a known semiconducting material whose band gap ranges from 2.15 to 2.70 eV [32]. It exhibit stunning optical, electronic, and magnetic properties [33] which leads toward consideration of this material for immersion into the PVDF. The CdO nanofillers have been embedded into the polymers to prepare the PVA nano composite and it has shown huge surprising applications. Rashmi et al. [34] have conducted experimental research on investing the mechanical and electrical properties evaluation of nano cadmium oxide polyvinyl alcohol composites. They found use of this material for microwave applications. Selvi et al. [35] have enumerated structural, optical, and thermal studies of PVA/CdO nano composite films and found use of this material for supercapacitors, gas sensors, electrochromic devices, and EMI shielding. Prabu et al. [36] have prepared and characterized CdO/PVA nanoparticles by precipitation method and their study revealed application of CdO/PVA material for paint pigments and cadmium coated bath. Chaitra Srikanth et al. [37] have published their findings relating to the effect of CdO–ZnO nanoparticles on the structural, electrical, and mechanical properties of PVA films. They found that CdO–ZnO desirably reinforce the material for nano composites. Hassan Karami et al. [38] have elucidated their PVA-based sol–gel synthesis and characterization of CdO–ZnO nanocomposites. They reported that PVA-based sol–gel pyrolysis method can be useful to synthesize the CdO–ZnO nano composites. Hence, through literature survey, we find a least contribution of scientific research work in the area of PVDF/CdO and yet more is to be investigated on this material in order to find its novel potential applications. Moreover, it is revealed that a combination of the CdO and transition metals is expected to introduce new dimensions to the CdO/PVDF nano composites. In current research work, study of CdO-PVDF matrix containing the transition metal

Zn nano-fillers has presented. The structural, electronic, and optical properties were explored. Many interesting results have been explored in this study which proposes the use of Zn:CdO-PVDF material as an excellent candidate for flexible mediums due to outstanding electronic and optical properties.

Computational and experimental method

Computational method

The density functional theory (DFT) [39] were employed to investigate the electronic and optical properties of the Zn-doped CdO. The full potential linearized augmented plane wave (FP-LAPW) is implemented in the Wien2k code [40]. For approximating the exchange–correlation, the Perdew-Burke-Erzernhof (PBE) generalized gradient approximation (GGA) in the Wien2k code [41]. A $2 \times 2 \times 2$ supercell configuration is constructed and Cd atoms are substituted with the Zn atoms and the impurity concentrations 12.5%, 25% and 50% are adjusted. The supercell is generated using the lattice constants $a = b = c = 4.738$ Å with the space group of Fm-3 m. The states ($4d^{10} 4p^6 5s^2$), ($2s^2 2p^4$), ($3p^6 3d^{10} 4s^2$) were considered as core states corresponding to the Cd, O and Zn atoms, respectively, whereas the remaining states are supposed frozen. The expansion value of angular momentum wave function is $l = 10$ while the spherically symmetric constant potential is assumed inside the muffin-tin sphere. For the atomic relaxations, the self-consistency criterion involving the minimum of energy and charge density convergence values of 10^{-4} eV and 10^{-2} C was used. The 400 k-points sampling using the Monkhorst–pack was used and ignored the relativistic effects in our computational study.

Experimental method

The beads of polyvinylidene difluoride (PVDF), zinc nitrate hexahydrate [$Zn(NO_3)_2 \cdot 6H_2O$], $Cd(CH_3COO)_2.2H_2O$ and ammonia solution were used for preparation of nanorods and polymer composite thin films. All the chemicals used have minimum 99.95% purity and were supplied by the Sigma-Aldrich, USA. All the precursors were of the analytical grade and were used without any purification.

Synthesis of the CdO and Zn:CdO nanorods

Zn substituted CdO nanorods having an average diameter of 50 nm to 100 nm were prepared through well-known co-precipitation methods. The required calculated weight percent amounts of starting precursors for CdO and Zn:CdO (12.5%, 25%, and 50% Zn) compositions were added in distilled water for 0.5 M solution each time for all compositions. The solutions were constantly stirred for mixing and heated at 50 °C on hot plate for 1 h. The ammonia solution was added drop wise until the pH was set to 9. The precipitates of white color substances were formed for each composition and wait to settle down for 2 h. These precipitates were washed

and filtered 5 times for removal of undissolved and excess reactants. The resultant precipitates were dried and calcined at 100 °C in an oven for 4 h in order to get the desired fine phase pure powders of metal oxides.

Synthesis of polymer composite thin films

The required amount of PVDF beads (1 wt%) was dissolved in distilled water along with un-doped and Zn-doped CdO nanorods (0.1 wt% to PVDF for each composition). These solutions were continuously stirred and heated at 40 °C until a thick gel of solutions were obtained. These resultant gels were spread on ultrasonically cleaned silicon (Si-100) substrates and spin coated at 500 and 4000 rpm for 10 and 30 s, respectively. These prepared thin films were dried by keeping in oven at 40 °C for 8 h. The thickness of each thin film was recorded approximately in the range of 300 ± 10 nm.

Characterizations

Morphology of nanorods and polymer composite thin films were observed using FEI Nova Nano-SEM 450 field emission scanning electron microscopy (FESEM). Elemental analysis was performed with Oxford X'Act energy-dispersive X-ray spectrometer (EDX). Optical response of polymer composite thin films were acquired using alpha-SE spectroscopic ellipsometry.

Results and discussions

Electronic properties and band structure

The occupancy of electrons over a specific energy range is understood as the density of states (DOS). The partial density of states (PDOS) and total density of states (TDOS) has been shown in Fig. 1 and have been plotted in energy range −5 to 5 eV. For the pure CdO, in the valence band the major contribution of Cd *d*-states and O *p*-states is seen at the Fermi level with least contribution of Cd *s*-states and O *s*-states [42, 43]. These contributions are observed in the energy range −3.7 to 0 eV in the valence band. But the TDOS plot of pure CdO contains prominent role of the O atoms in the valence band. However, in the conduction band, the role of Cd *s*-states and O *p*-states is clearly remarked at the higher energies. On the other hand, the effect of Zn doping causes appreciable changes in the CdO and the density of states of the Zn-doped CdO have been expressed in Fig. 1b–d. The contributions of the (*s*, *p*, *d*) states is found in the energy range −3.8 to −0.01 eV in the valence band. The dominance of the Cd *d*-states, O *p*-states and Zn *d*-states may be easily observed in the valence band along with minimum participation of the Cd *s*-states, O *s*-states, and Zn *s*-states. The significant improvement in role of dopant (Zn) *d*-states along with increasing its concentrations in the host CdO may be noted at the maxima of the valence band. Localization of the Zn *3d* states electrons at the Fermi level, enables the chances of conductivity enhancement in the Zn:CdO material. It is pertinent to mention here that increasing the
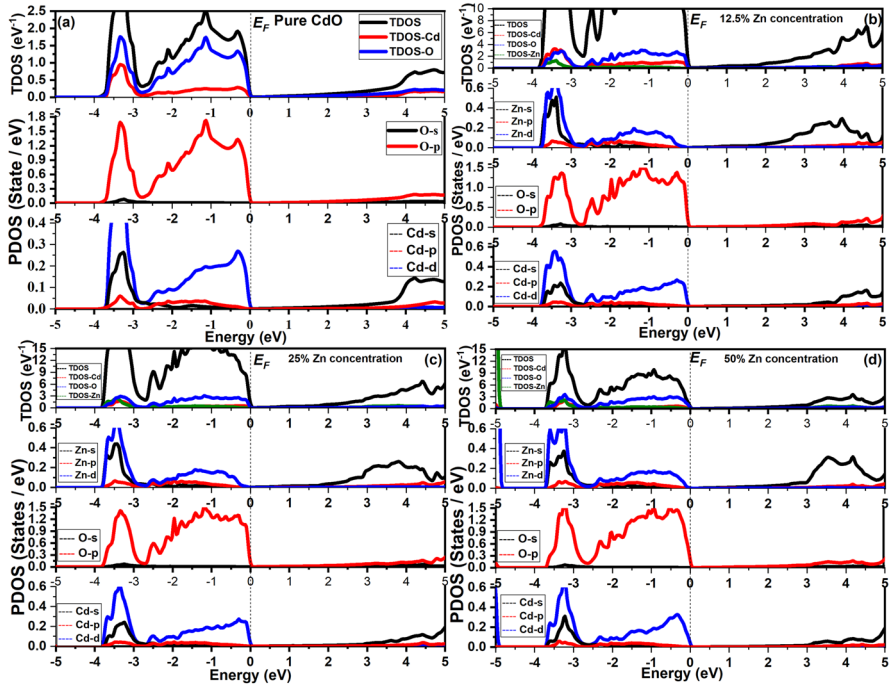
Fig. 1 TDOS and PDOS of pure and Zn substituted CdO **a** Pure CdO, **b** 12.5% Zn in CdO, **c** 25% Zn in CdO, and (d) 50% Zn in CdO

Zn concentrations, activates the involvement and participation of the increased atomic interactions and likewise, it activates the maximum contribution of the impurity $3d$ electrons in the vicinity of the Fermi level. In addition to the PDOS behavior, the total density of states of the Zn-doped CdO reflects the leading role of the oxygen atoms. Moreover, p-d hybridization due to active involvement of the Zn d-states and O p-states is observed which significantly improves the electronic properties of CdO after dopant addition.

Optical properties of Zn:CdO material

The transition of electrons and recombination rate affects the optical properties of materials. The study of the optical properties illustrate potential uses of the materials in various technological fields. Optical properties are characterize in terms of the optical constants which are calculated via dielectric function $\varepsilon(\omega)$. Absorption coefficient may be calculated from the real ($\varepsilon_r(\omega)$) and imaginary part ($\varepsilon_i(\omega)$) of the dielectric constant [44],

$$\alpha(\omega) = \sqrt{2}\left[\sqrt{\varepsilon_r^2(\omega) + \varepsilon_i^2(\omega)} - \varepsilon_r(\omega)\right]^{1/2}$$

The absorption coefficient of pure CdO and Zn-doped CdO has been shown in Fig. 2a. The optical absorption has been studied in the energy range 0–7 eV. The absorption of the pure CdO gradually increases and obtains maximum absorption at 6.5 eV (~ 190 nm). However, an extended absorption hump is noticed at 4.94 eV (~ 250 nm) but beyond 6.5 eV, the absorption of pure CdO becomes constant for higher energy values. This broad absorption edge may correspond to the feature of the CdO nanoparticles as reported in [45]. The impurity addition into the CdO in a specific proportion (12.5%, 25%, 50%) clearly changes the absorption spectrum but shows similar trends (increasing and decreasing) as of pure CdO. The absorption maxima corresponding to the various Zn concentrations exist at energies: 12.5% ~ 6.43 eV, 25% ~ 6.44 eV and 50% ~ 6.94 eV. The blue shift is observed upon increasing the Zn contents and is attributed to the optical band gap value [46]. This blue shift may be connected to the size quantization which occurs owing to electron localization (as observed in DOS plots in (Fig. 1) in the material volume. Moreover, blue shift in absorption spectra may be related to the morphology of the Zn:CdO as confirmed in experimental study [47]. The emergence of blue shift in the absorption spectrum resembles with the works reported by Kumar et al. [46] and Kavakebi et al. [48]. Shifting of the absorption onsets with addition of various Zn concentrations may be referred to the quantum confinement effects and it causes presence of free states in the conduction band. However, broadening of the absorption peaks is due to impurity concentrations and is the result of the impurity interband transitions [44]. We observed zero absorption for the pure CdO and Zn-doped CdO in the low energy range 0–0.92 eV which indicates that no energy is absorbed at this frequency range. Absorption maxima are observed in the UV range which decreases in the near IR region. The oscillatory trends are more evident for the highest Zn concentrations (50%) and are related to absorption of light at different frequencies due to upgraded surface morphologies. Furthermore, the scope of this material may be extended by
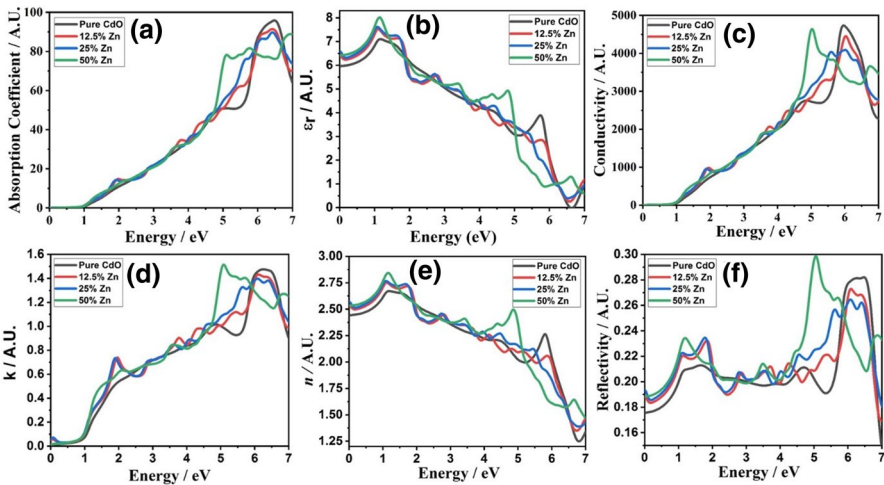

Fig. 2 Trend of **a** Absorption coefficient, **b** Real epsilon, **c** Optical conductivity, (d) extinction, (e) Refractive index, and (f) Reflectivity with energy for un-doped and Zn-doped CdO

adjusting the impurity concentrations for the purpose of using them in the PVDF host matrix.

The dielectric constant ($\varepsilon(\omega)$) of the materials is an important optical constant because it helps in permitting the electromagnetic field through the material. The dielectric constant ($\varepsilon(\omega) = \varepsilon_r(\omega) + i\varepsilon_i(\omega)$.) is composed of real ($\varepsilon_r(\omega)$) and imaginary parts ($\varepsilon_i(\omega)$). The real part is calculated through the imaginary part via the Krammers–Kroning transformation while the imaginary part is achieved by the direct solution of the many body electron wave function [44],

$$\varepsilon_r(\omega) = 1 + \frac{2}{\pi}\rho_0 \int\limits_0^\infty \frac{\omega' \varepsilon_i(\omega)}{\omega'^2 - \omega^2} d\omega$$

The real part of the dielectric constant of pure and Zn-doped CdO has been calculated in energy range 0–7 eV and is shown in Fig. 2b. The $\varepsilon_r(\omega)$ for the impurity doped and undoped CdO have almost similar trends (increasing and decreasing) but the dielectric maxima occurs at different frequency (energy) for each case. For the pure CdO, the maximum value of $\varepsilon_r(\omega)$ found at 1.13 eV and for higher energy values, it becomes almost constant. Impurity addition increases the dielectric constant values and dielectric maxima corresponding the 12.5%, 25%, and 50% Zn concentrations are 7.6 (~ 1.1 eV), 7.66 (~ 1.0 eV), and 8.0 (~ 1.14 eV), respectively. A notable difference in the dielectric response of higher Zn concentration is observed that in the 1.14–5.82 eV energy range, the $\varepsilon_r(\omega)_{50\%}$ shows a steady decrease with some oscillations but the $\varepsilon_r(\omega)$ for the rest of the cases decreases of 1.0–6.63 eV. However, the values of the static dielectric constant ($\varepsilon_r(0)$) are: 5.94 ~ pure CdO [49], 6.46 ~ 12.5%, 6.62 ~ 25%, and 6.45 ~ 50%. An increase in dielectric constant is with effect of impurity and it is due to increase in loss factor which increase with increase in frequency (energy) [44]. Moreover, the dielectric response for the three Zn concentrations is same in the low energy range 0–1 eV and exhibit higher $\varepsilon_r(\omega)$ values than pure CdO which are due to the presence of all type of polarizations. These polarizations may disappear for the higher energy values. The polarizations which cannot catch up with variations in the electromagnetic field results a decrease in the $\varepsilon_r(\omega)$ along with increase in frequency [50].

Optical conductivity ($\sigma(\omega)$) of the materials is the redistribution of charges upon interaction of the material with the electromagnetic radiations. The conductivity is calculated in terms of the dielectric constant using the formula [44],

$$\sigma(\omega) = -i\frac{\omega}{4\pi}|\varepsilon(\omega) - 1|.$$

The conductivity of pure and Zn-doped CdO has been shown in Fig. 2c where the conductivity variations are recorded in 0–7 eV energy range. The conductivity rises for the pure CdO and Zn:CdO materials beyond 0.92 eV. It signifies that pure and Zn-doped CdO does not yield any response to electromagnetic field in the energy range 0–0.92 eV as obvious in absorption plots (Fig. 2a). The maximum conductivity of pure CdO has been observed at 5.95 eV and becomes constant for higher energy values. Conductivity traits for the Zn:CdO material shows distinct variations

in the 4.2–6.7 eV. However, the conductivity maxima corresponding to various Zn concentrations are obtained at energies; 6.02 ∼. 12.5%, 6.01 ∼ 25%, and 5.02 50%. The conductivity peaks represent the deep penetrations of electromagnetic waves inside the material and likewise, depicts the higher optical conductivity. Conductivity peaks appears due to the impurity inter-band transitions. The conductivity peaks are shifted due to *p-d* hybridization as observed in the DOS plots (Fig. 1). So, the localization of states are responsible for the conductivity behavior of the Zn:CdO material. Hence, it is worth to mention here that conductivity well-defined peaks are observed in the UV region which enable uses of Zn:CdO for UV optoelectronics [51].

In optics, the extinction coefficient (*k*) of the materials as it helps us to physically describe the absorption of radiations for a particu ∼ lar frequency (energy). It is calculated using the formula [44],

$$k = \frac{\lambda\alpha}{4\pi}.$$

The extinction coefficient has been recorded in the energy range 0–7 eV and a clear resemblance may be observed between the plots 2(a) and 2(d). The constant rise and fall in the extinction trends for the pure and Zn-doped CdO is noted and it may be due to the light absorption at the grain boundaries. The increase in *k* values along with increase in corresponding energy values is the result of quantum confinement effects. The maximum extinction for the pure CdO is obtained at 6.3 eV which decreases beyond 6.3 eV and becomes constant for higher energy values [52]. Doping causes emergence of *k* peaks in the low energy region 0–0.34 eV and it may be due to quantum confinement effects which are more pronounced upon increasing number of atoms in the Zn:CdO material at various Zn concentrations. However, extinction maxima for various Zn concentrations are obtained at energies; 6.07 s ∼ 12.5%, 6.06 ∼ 25%, and 5.08 ∼ 50%. The extinction edges indicate the good absorption and represent deep penetration of electromagnetic waves inside the material. Moreover, the density of states of electrons available around the Fermi level is the reason for the extinction peaks composition and such states are the result of impurity addition. The larger values of *k* represent the absorption at defect sides which causes maximum attenuation [44]. Our DFT calculated *k* values (0–0.03) are lower than the extinction values for pure CdO as reported in [53, 54] and the difference in extinction values are due to assumptions of theory and experiment.

The behavior of light can be understood by studying the refractive index (*n*) which is of course an important factor in optical communication and optoelectronic devices. Figure 2e is a representation of the refractive indices of the pure CdO and Zn:CdO material. Refractive indices variations have been studied in the energy range 0–7 eV and in general, an increasing and decreasing trend of refractive indices has been noticed. For the pure CdO, the maximum value (2.67) of refractive index is obtained at 1.16 eV and for the higher energy values, the *n* becomes constant. Upon adding the Zn impurity, the refractive index is found to be increased. The maximum values of the refractive indices for various Zn concentrations are; 2.7 ∼ 12.5%, 2.76 ∼ 25%, and 2.85 ∼ 50%. The variations in *n* are associated with the dispersion of light as it deeply permeates inside the material. Interaction of various atoms inside the materials along with dopant different concentrations results change in the refractive index of the selected materials. The static values of the refractive indices for

our selected materials are; 2.44 ~ pure CdO, 2.52 ~ 12.5%, 2.57 ~ 25%, and 2.52 ~ 50%. The refractive index first increases and then decreases as Zn concentrations are further increases. It may be due to change in morphology and stoichiometry [55]. Our DFT calculated values of refractive indices matches with the reported works [52, 56] but differ from the works [49, 57]. The prominent changes in *n* are observed in the UV region and for higher energies; it becomes constant for all the materials. The *n* values decreased in denser mediums and reason for lowering of *n* values may be associated with the DOS plots (Fig. 1) because of localization of impurity states at the Fermi level.

The reflectivity ($R(\omega)$) of pure and Zn-doped CdO has been shown in Fig. 2f and is calculated using the formula [44],

$$R(\omega) = \left[\frac{\sqrt{\varepsilon_1(\omega) + i\varepsilon_2(\omega)} - 1}{\sqrt{\varepsilon_1(\omega) + i\varepsilon_2(\omega)} + 1} \right]^2$$

The reflectivity of pure CdO increases with increase in energy (eV) and have maximum reflectivity at 6.47 eV. It means that at this energy, there is zero absorption of the electromagnetic radiations inside the material [58]. However, reflectivity maxima for the various concentrations of dopant (Zn) are obtained at energies; 6.07 eV ~ 12.5%, 6.07 ~ 25%, and 5.0 eV ~ 50% [49]. The reflectivity humps are observed in the UV region and for the highest Zn concentration, reflectivity is maximum. Reflectivity peaks emerged because of impurity interband transitions from valence to conduction band. In comparison with pure CdO, the impurity added CdO shows reflectivity peaks in the low energy region 0–2 eV and they appear due to multiple reflections inside the materials.

Morphology and elemental composition of Zn:CdO-PVDF

The morphology of the polymer composites and synthesized nanoparticles was examined by the FEI Nano-SEM 450 field emission scanning electron microscopy (FESEM) using the built in scanning transmission electron microscope (STEM) and high resolution through lens (TLD) detector. Figure 3 presents the FESEM micrographs of synthesized un-doped and Zn-doped CdO nano-rods. CdO nano-rods (Fig. 3a) contain the approximate average width size of less than 100 nm with uniform sizes of length and shape. The size of nano-rods for Zn substituted CdO (Fig. 3b–d) decreased in length with slight variation in shape. The cubic shaped morphology of rods seems increasing in the higher contents of Zn in CdO. EDX spectra (Fig. 4) confirm the phase purity and presence of expected elemental contents (Cd, O, and Zn) in relevant compositions.

Figure 5 contains the FESEM micrographs of Zn:CdO nanorods containing PVDF polymer composite thin films along with their EDX spectra. Fiber like composite morphology is observed for the PVDF which somehow seems disturbed by the addition of CdO, where rod-like or acicular morphology is witnessed. This rod-like distribution is not uniform over the surface and changed
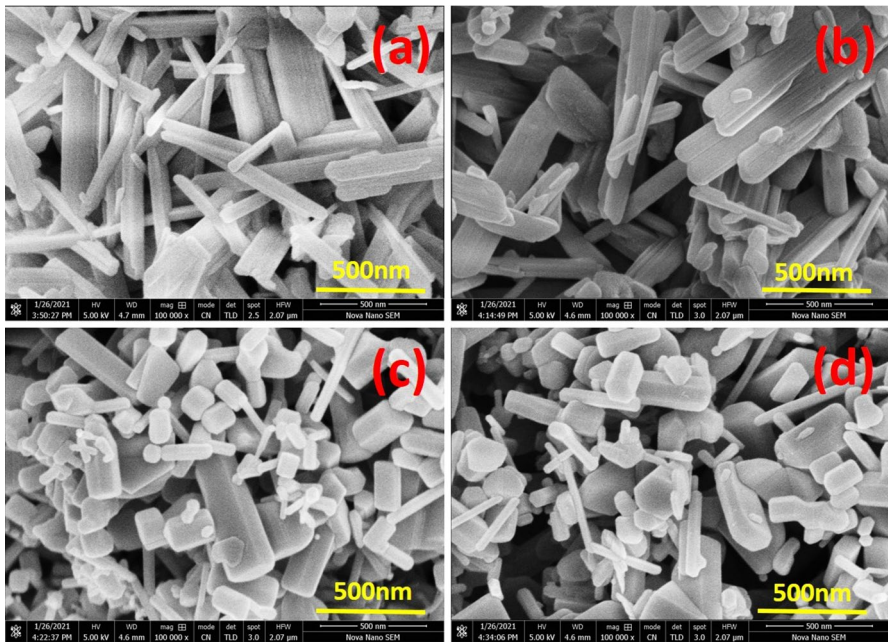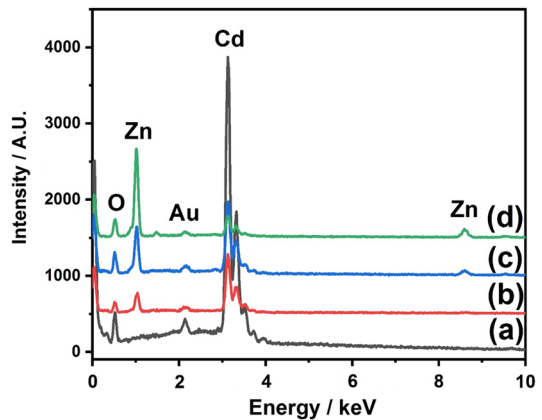
Fig. 3 FESEM micrographs of prepared **a** Pure CdO, **b** 12.5% Zn in CdO, **c** 25% Zn in CdO, and **d** 50% Zn in CdO nanorods

Fig. 4 EDX spectra of prepared **a** Pure CdO, **b** 12.5% Zn in CdO, **c** 25% Zn in CdO, and **d** 50% Zn in CdO nanorods

after adding Zn contents. The addition of Zn contents into the CdO-PVDF matrix changes the dense rod-like morphology to uniform for higher Zn concentrations (Fig. 5). Micrographs of all compositions depict the uniform distribution of nanorods in PVDF matrix. The sharp carbon and fluorine contents in EDX spectra are associated with the PVDF polymer matrix and elemental contents of Cd, O and Zn associated with the nano-rod compositions.
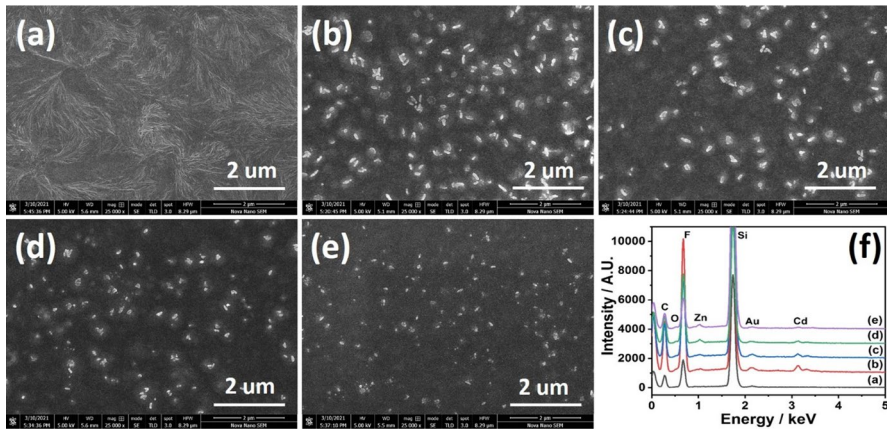
Fig. 5 FESEM micrographs of **a** PVDF, **b** CdO-PVDF, **c** 12.5%Zn:CdO-PVDF, **d** 25%Zn:CdO-PVDF, **e** 50%Zn:CdO-PVDF, and **f** EDX spectra of thin films

Optical properties of Zn:CdO-PVDF composites

The spectroscopic Ellipsometry were employed to evaluate the optical properties of the synthesized polymer nano-composites. A UV–Viz spectrophotometer has been used to estimate the experimental values of the optical constants of the Zn:CdO-PVDF composites. The absorption spectra along with the estimation of the band gap were found using the Tauc plot for the pure and transition metal oxide nanoparticles PVDF-CdO and are expressed in Fig. 6a. It is interesting to note that these composites show distinct absorption edges in the visible region. Absorption spectrum of the pure PVDF shows a
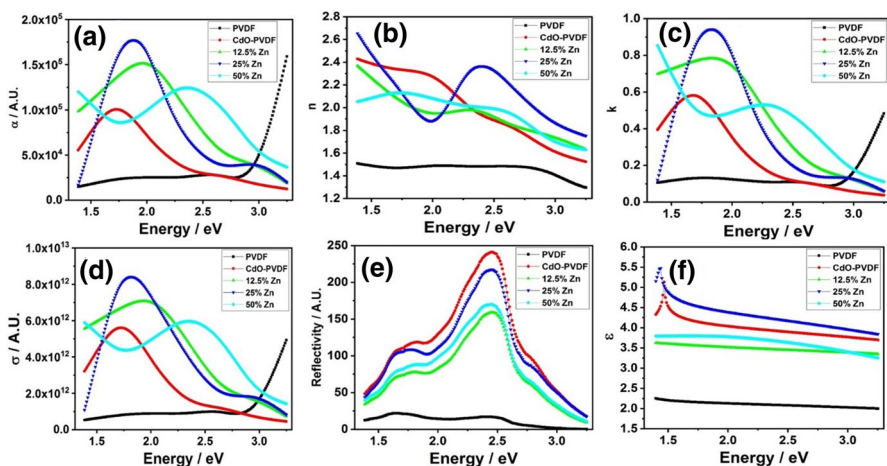

Fig. 6 Trend of **a** Absorption coefficient, **b** Real epsilon, **c** Optical conductivity, **d** extinction, **e** Refractive index, and **f** Reflectivity with energy for PVDF and Zn:CdO nanorods containing PVDF thin films

flat absorption characteristic which however, rises beyond 2.89 eV because of spectral features [59]. The extended absorption shoulder indicates different scattering mechanisms due to fiber like morphology and may further be destined to strong convolution effects [60]. The pure PVDF has lower absorption coefficient but increases significantly due to addition of Zn:CdO. The PVDF absorption spectrum becomes rich with addition of the CdO and Zn:CdO. It indicates that it is sensitive to morphological changes (Fig. 5) in the host PVDF matrix. Because of the increasing acicular morphology along with smaller diameters, the absorption spectrum shows improvements in the visible region [61]. The CdO-PVDF matrix without and with selected Zn concentrations (12.5%, 25%, and 50%), shows absorption maxima at energies 1.72 eV (~ 720 nm), 1.95 eV (~ 635 nm), 1.87 eV (~ 663 nm) and 2.35 eV (~ 527 nm), respectively. The linearity in the absorption spectrum of CdO-PVDF and with Zn concentrations may emerge due to the fact that for higher energies, the behavior of polymer is like insulator for the CdO [59]. The absorption peaks in the CdO plus Zn added PVDF indicate the aggregation of the CdO nanoparticles and is the effect of adding various Zn concentrations to the host matrix. It is interesting fact to mention that no absorption in the CdO-PVDF with and without Zn concentrations was found in the absorption spectra at the high energies which enable these selected materials to be potentially used in the visible range devices. However, the non-uniform distribution of the absorption spectrum of all the materials appears due to presence of two phases (CdO and Zn concentrations) in the host PVDF matrix. The optical band gap analysis is very important to present and hence optical band gap discussion were extracted of the synthesized polymer composites as calculated using the Tauc plots [62],

$$(\alpha h v)^n = B(h v - E_g).$$

where the parameters α, B, hv, and E_g are called the absorption coefficient, interband transition probability parameter, photon energy, and optical band gap, respectively. The optical band gaps corresponding to the polymer composites were extracted by extra plotting the tangent on the X-axis and have been shown in Fig. 7. The optical band gap of the PVDF is calculated to be 2.9 eV [63, 64] while the optical band gap after adding nano fillers to PVDF are; 1.22 eV ~ CdO-PVDF, 1.14 eV ~ 12.5%Zn, 1.41 eV ~ 25%Zn, and 1.66 eV ~ 50%Zn. The lower value of the optical band gap for the 12.5% appears due to local cross linking between the interpenetrating

Fig. 7 Tauc plot for estimation of band gap of **a** PVDF, **b** CdO-PVDF, **c** 12.5% Zn in CdO-PVDF, **d** 25% Zn in CdO-PVDF, and **e** 50% Zn in CdO-PVDF thin films
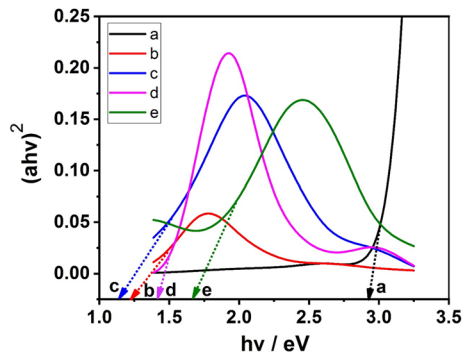
Zn:CdO-PVDF nanocomposites. The nanoparticles of the Zn:CdO coagulated with the interpenetrating PVDF and causes decrease in the molecular mobility. It consequently decreases the optical band gap [63, 65].

The refractive index (n) of the PVDF and polymer composite has been shown in Fig. 6b. The refractive indices spectra have been studied in the energy range 1.3–3.3 eV and it is clear that the addition of the Zn:CdO contents in the PVDF matrix makes the refractive indices higher. The variations in the refractive indices are very clear at the higher wavelength (low frequency) but diminish for the lower wavelength as may be seen by the constant trend in the n plots. The refractive index of the PVDF matrix as obtained through our experimental study is 1.5 and it resemble with the work reported in [66–68]. However, the maximum values of the refractive indices for the PVDF composites are; 2.4 ~ CdO-PVDF, 2.37 ~ 12.5%Zn, 2.67 ~ 25%Zn, and 2.14 ~ 50%Zn. The refractive index has a great dependence on the nature of the surface of material (smooth or rough) [69]. The surface as observed through FESM images shows a kind of rough morphology for the CdO-PVDF without and with 12.5% and 25% Zn concentrations (Fig. 5b–d). Therefore, exhibit higher n values in comparison with pure PVDF (Fig. 5a) and CdO-PVDF with 50% Zn concentration (Fig. 5e) where surfaces show smaller roughness. Hence, smaller roughness of the surfaces enables the better optical coupling between the interacting light and sample. The improvement in the refractive index is dependent on the transition metal oxides and likewise, the optical properties of the Zn:CdO-PVDF polymer composite may be extended to optoelectronic and optical devices.

The variations in the extinction coefficient (k) of the Zn:CdO-PVDF has been recorded in energy range 1.3–3.3 eV and are demonstrated in Fig. 6c. A constant extinction trend is observed for the PVDF which shows exponential rise at 2.86 eV [70]. However, extinction maxima for our selected materials are obtained at energies; 1.6 eV ~ CdO-PVDF, 1.83 eV ~. 12.5%Zn, 1.82 eV ~ 25%Zn, and 1.37 eV ~. 50%Zn. The variations in the k trends for selected materials have dependence on the surface morphology. The variations in the surface morphologies of materials have been discussed in Sect. 3.3. In general, the non-uniformity of the materials surfaces greatly enhances the extinction coefficient and in current study, the higher k values are noticed for the CdO-PVDF at 25% Zn concentration (Fig. 5d), confirming the better performance of nano-rods or acicular morphology with interaction of light [71]. It is obvious that extinction coefficient increases with increase in energy and the higher extinction values are noted in the visible region. The higher extinction values indicate the higher absorption at that energy value.

The optical conductivity of the Zn:CdO-PVDF materials has been shown in Fig. 6d. The optical conductivity of the materials shows appreciable improvement with the varying Zn concentrations. The conductivity of the materials strongly depends on the surface morphology as the quality of the surface helps in absorbing the light perfectly. The fiber like morphology causes light scattering and hence lower absorption is observed for PVDF. But the acicular or rod-like morphology helps in improving absorption for the CdO-PVDF and Zn:CdO-PVDF. However, an appreciable enhancement in optical conductivity is noted for Zn:CdO-PVDF at 25% Zn concentration. The conductivity of the PVDF is almost constant for the low energy values but rises sharply after 2.82 eV. But the maximum conductivity of the materials is obtained at energies;

1.71 eV ~ CdO-PVDF, 1.94 ~ 12.5%, 1.81 eV ~ 25%, and 2.38 eV ~ 50%. The conductivity maxima are observed in the visible region but decrease in the IR and vanish in the UV region. The increasing Zn concentrations lead to enhancement of the optical conductivity. The increase in the charge transfer excitations inside the materials leads to the substantial increase in conductivity and it signifies the use of this material for the optoelectronic devices operating in the visible region.

The reflectivity of the Zn:CdO-PVDF materials has been shown in Fig. 6e where the reflectivity variations are observed in the 1.3–3.3 eV. The reflectivity of the PVDF shows constant rise and fall with increase in energy and maximum reflectivity is obtained at 1.63 eV. However, reflectivity trends are significantly changed with various Zn concentrations. The reflectivity maxima for our selected PVDF materials are obtained at energies; 2.45 eV ~ CdO-PVDF, 2.45 eV ~ 12.5%Zn, 2.44 ~ 25%Zn, and 2.44 eV ~ 50%Zn. These reflectivity changes may further be connected to the surface morphology and in current study, evident changes in reflectivity have been observed. The dense rod-like morphology appearing in the CdO-PVDF causes maximum reflections (lower absorption) with least scattering. But the morphological variations help in switching the reflectivity behavior of selected materials and because of the non-uniform rod-like morphology in the Zn:CdO-PVDF at 25% Zn, lower reflectivity is observed. Moreover, the notable reflectivity peaks are observed in the visible region and the high reflectivity of the PVDF composites extend the scope of these composite for the field of solar photovoltaic back panel applications.

The real part of the dielectric constant of Zn:CdO-PVDF composites has been shown in Fig. 6(f) and its variations are recorded in the 1.3–3.3 eV. The dielectric trend for the PVDF material is almost constant and its maximum value (2.25) is obtained at an energy of 1.38 eV [59]. However, the ε_r maximum values for the CdO-PVDF, 12.5%, 25%, and 50% Zn are; 5.1 1.47 eV, 3.6 ~ 1.39 eV, 5.4 ~ 1.43 ~ eV, and 3.7 ~ 1.39 eV, respectively. The lower dielectric constant is observed for PVDF and exhibit maximum value for 25% (Zn:CdO-PVDF material). The high dielectric values observed at low frequency is due to the interfacial phenomenon occurring in the sample [37] and decreases with increase in frequency of the applied field. At the high frequencies, the polymer nanocomposites behave like a semiconductor [72]. The morphological variations in the selected materials may be responsible for the improvement in dielectric properties and dispersion. A particular dielectric trend is observed corresponding to each morphology (Fig. 5). The presence of the rod-like morphology induces the dipole polarization and enhancement of trapped charge carriers. These polarization effects are highly observed in the Zn:CdO-PVDF with 25% Zn concentration where higher dielectric constant is noted. The high dielectric constant of the PVDF composites enables the use of these composites in the dielectric spectroscopy, photo displays, spintronics, and optoelectronics.

Conclusion

In the current study, the electronic and optical properties of the Zn:CdO-PVDF polymer composite thin films were investigated. At the initial stage, the optical response of the Zn substituted CdO were calculated using the Wien2k code. Then pure and

Zn-doped CdO nanorods were prepared through the co-precipitation method. Then, uniform thin films of Zn:CdO-PVDF were deposited and performed its characterization. The fiber like morphology of the pure PVDF is noticed while the rod-like morphology is observed for the Zn:CdO-PVDF nanocomposites. Elemental composition analysis confirmed the presence of expected elements in dissolved amounts in each composition. Optical response of polymer composite thin films depicts the interesting distinct absorption edge in visible region. The band gap presents a significant variation for un-doped and Zn-doped CdO nano-rods containing PVDF thin films.

Declarations

Conflict of interest The authors declare that they have no known competing financial interests or personal relationships that could have appeared to influence the work reported in this paper.

References

1. Maksoud MA et al (2021) Advanced materials and technologies for supercapacitors used in energy conversion and storage: a review. Environ Chem Lett 19(1):375–439
2. Soares PI et al (2021) Design and engineering of magneto-responsive devices for cancer theranostics: nano to macro perspective. Prog Mater Sci 116:100742
3. Chen L et al (2021) Polymer informatics: current status and critical next steps. Mater Sci Eng R: Rep 144:100595
4. Liu H et al (2021) Electrically conductive coordination polymers for electronic and optoelectronic device applications. J Phys Chem Lett 12(6):1612–1630
5. Li D, Yu G (2021) Innovation of materials, devices, and functionalized interfaces in organic spintronics. Adv Funct Mater 31:2100550
6. Oladele IO, Omotosho TF, Adediran AA (2020) Polymer-based composites: an indispensable material for present and future applications. Int J Polym Sci 2020:1–12
7. Pradeesh G et al (2021) Synthesis of single-phase MoO_3-nanoparticles using various acids for the fabrication of n-MoO_3/p-Si junction diode. J Inorg Organomet Polym Mater 31(6):2638–2647
8. Srivastava A et al (2015) Investigations on structural, mechanical, and dielectric properties of PVDF/ceramic composites. J Eng 2015:1–9
9. Jylhä L et al (2005) Microstructure-based numerical modeling method for effective permittivity of ceramic/polymer composites. J Appl Phys 97(10):104104
10. Ambrosio R et al (2018) Polymeric nanocomposites membranes with high permittivity based on PVA-ZnO nanoparticles for potential applications in flexible electronics. Polymers 10(12):1370
11. Li Y et al (2011) Large dielectric constant and high thermal conductivity in poly (vinylidene fluoride)/barium titanate/silicon carbide three-phase nanocomposites. ACS Appl Mater Interfaces 3(11):4396–4403
12. Wang Z et al (2017) Ultrahigh dielectric constant and low loss of highly-aligned graphene aerogel/poly (vinyl alcohol) composites with insulating barriers. Carbon 123:385–394
13. Sharafkhani S, Kokabi M (2020) Ultrathin-shell PVDF/CNT nanocomposite aligned hollow fibers as a sensor/actuator single element. Compos Sci Technol 200:108425
14. Zou Y et al (2020) Flexible and robust polyaniline composites for highly efficient and durable solar desalination. ACS Appl Energy Mater 3(3):2634–2642
15. Zhang Q et al (2002) An all-organic composite actuator material with a high dielectric constant. Nature 419(6904):284–287
16. Koerner H et al (2004) Remotely actuated polymer nanocomposites—stress-recovery of carbon-nanotube-filled thermoplastic elastomers. Nat Mater 3(2):115–120

17. Pazhamalai P et al (2020) Free-standing pvdf/reduced graphene oxide film for all-solid-state flexible supercapacitors towards self-powered systems. Micromachines 11(2):198

18. Chen X, Han X, Shen QD (2017) PVDF-based ferroelectric polymers in modern flexible electronics. Adv Electron Mater 3(5):1600460

19. Kang G-D, Cao Y-M (2014) Application and modification of poly (vinylidene fluoride)(PVDF) membranes–a review. J Membr Sci 463:145–165

20. Zhang Y et al (2014) PVDF–PZT nanocomposite film based self-charging power cell. Nanotechnology 25(10):105401

21. Ribeiro C et al (2018) Electroactive poly (vinylidene fluoride)-based structures for advanced applications. Nat Protoc 13(4):681

22. Parthasarathy V et al (2020) Evaluation of mechanical, optical and thermal properties of PVA nanocomposites embedded with Fe 2 O 3 nanofillers and the investigation of their thermal decomposition characteristics under non-isothermal heating condition. Polym Bull 78:2191–2210

23. Mallkpour S, Lormahdiabadi M (2020) Production of the ZnO-folic acid nanoparticles and poly (vinyl alcohol) nanocomposites: investigation of morphology, wettability, thermal, and antibacterial properties. J Polym Res 27(9):1–16

24. Abed RN et al (2021) Enhancing optical properties of modified PVC and Cr 2 O 3 nanocomposite. Trans Electr Electron Mater 22(3):317–327

25. Abed R, Abed A, Yousif E (2021) Carbon surfaces doped with (Co3O4-Cr2O3) nanocomposite for high-temperature photo thermal solar energy conversion via spectrally selective surfaces. Progr Color, Colorants Coat 14(4):301–315

26. Abed RN et al (2021) New coating synthesis comprising CuO: NiO/C to obtain highly selective surface for enhancing solar energy absorption. Polym Bull 78(1):433–455

27. Abed RN et al (2021) Optical properties of PVC composite modified during light exposure to give high absorption enhancement. J Non-Cryst Solids 570:120946

28. Abed R et al (2020) High performance thermal coating comprising (CuO: NiO) nanocomposite/C spectrally selective to absorb solar energy. Progress in Color, Colorants Coat 13(4):275–284

29. Al-Azzawi ZM et al (2021) Influence of nano silicon carbide (SiC) embedded in poly (Vinyl Alcohol)(PVA) lattice on the optical properties. Silicon. https://doi.org/10.1007/s12633-021-01325-8

30. Bakhtiari SSE et al (2019) Chitosan/MWCNTs composite as bone substitute: physical, mechanical, bioactivity, and biodegradation evaluation. Polym Compos 40(S2):E1622–E1632

31. Sekar AD et al (2018) Photocatalytic degradation of naphthalene using calcined FeZnO/PVA nanofibers. Chemosphere 205:610–617

32. Ueda N et al (1998) Band-gap widening of CdO thin films. J Appl Phys 84(11):6174–6177

33. Hoat D et al (2020) Structural, electronic and optical properties of CdO monolayer and bilayers: stacking effect investigations. Superlattices Microstruct 145:106644

34. Rashmi S et al (2018) Structural mechanical and electrical property evaluation of nano cadmium oxide polyvinyl alcohol composites. Int J Plast Technol 22(1):41–55

35. Selvi J, Mahalakshmi S, Parthasarathy V (2017) Synthesis, structural, optical, electrical and thermal studies of poly (vinyl alcohol)/CdO nanocomposite films. J Inorg Organomet Polym Mater 27(6):1918–1926

36. Prabu K, Anbarasan P, Janarthanan S (2014) Preparation characterization of CDO/PVP nanoparticles by precipitation method. Asian J Eng Appl Technol 2:66–70

37. Srikanth C et al (2019) The effect of CdO–ZnO nanoparticles addition on structural, electrical and mechanical properties of PVA films [J]. AIMS Mater Sci 6(6):1107–1123

38. Karami H et al (2010) PVA-based sol–gel synthesis and characterization of CdO–ZnO nanocomposite. J Cluster Sci 21(1):1–9

39. Schwarz K, Blaha P, Madsen GK (2002) Electronic structure calculations of solids using the WIEN2k package for material sciences. Comput Phys Commun 147(1–2):71–76

40. Slater JC (1937) Wave functions in a periodic potential. Phys Rev 51(10):846

41. Perdew JP, Burke K, Ernzerhof M (1996) Generalized gradient approximation made simple. Phys Rev Lett 77(18):3865

42. Pius JJ, Louis N, Amalraj A (2016) Band structure, density of states, structural phase transition and metallization in CdO Under high pressure. Orbital Electron J Chem 8(6):325–328

43. Das A et al (2020) Orbital hybridization-induced band offset phenomena in Ni x Cd 1–x O thin films. Nanoscale 12(2):669–686

44. Khan MJI et al (2021) Effect of Zn doping on electronic structure and optical properties zinc-blende GaN (A DFT+ U insight). Commun Theor Phys 73(3):035701

45. Jeejamol D et al (2018) Optimization of CdO nanoparticles by Zr 4+ doping for better photo-catalytic activity. J Mater Sci: Mater Electron 29(1):97–116

46. Kumar P et al (2020) Optical and surface properties of Zn-doped CdO nanorods and antimicrobial applications. Colloids Surf A: Physicochem Eng Aspects 605:125369

47. Chate P, Sathe D, Hankare P (2013) Electrical, optical and morphological properties of chemically deposited nanostructured tungsten disulfide thin films. Appl Nanosci 3(1):19–23

48. Kavakebi M, Jamali-Sheini F (2018) Ultrasonic synthesis of Zn-doped CdO nanostructures and their optoelectronic properties. Trans Nonferrous Metals Soc China 28(11):2255–2264

49. Mustafa DAS, Al-Rawi RIM (2018) Structural and optical properties for Zn-doped CdO thin films prepared by pulse laser deposition. Iraqi J Sci 58:839–846

50. Kirby S (2009) Electronic and optical properties of oxide thin films. Doctoral dissertation, Cornell University

51. Bairy R et al (2019) Role of Zn in tuning the band gap, surface morphology, photoluminescence and optical nonlinearities of CdO nanostructures for photonic device applications. Mater Res Express 6(9):096447

52. Choi S et al (2010) Complex dielectric function and refractive index spectra of epitaxial CdO thin film grown on r-plane sapphire from 0.74 to 6.45 eV. J Vac Sci Technol B Nanotechnol Microelectron Mater Process MeasPhenom 28(6):1120–1124

53. Raaif M, Mohamed S (2017) The effect of Cu on the properties of CdO/Cu/CdO multilayer films for transparent conductive electrode applications. Appl Phys A 123(6):441

54. Aydogu S, Çoban MB, Cabuk G (2017) Influence of doping fluorine on the structural, surface morphological and optical properties of CdO films. Appl Phys A 123(6):409

55. Sharma P, Sharma V, Katyal SC (2006) Variation of optical constants in Ge10Se60Te30 thin film. Chalcogenide Lett 3(10):73–79

56. Jandow N et al (2019) Theoretical and experimental investigation of structural and optical properties of lithium doped cadmium oxide thin films. Mater Res Express 6(11):116434

57. Anitha M et al (2018) Effect of Zn doping on structural, morphological, optical and electrical properties of nebulized spray-deposited CdO thin films. Appl Phys A 124(8):1–13

58. Sahbeni K et al (2020) Effect of CdO ratios on the structural and optical properties of CdO–TiO 2 nanocomposite thin films. J Mater Sci: Mater Electron 31(4):3387–3396

59. Devi PI, Ramachandran K (2011) Dielectric studies on hybridised PVDF–ZnO nanocomposites. J Exp Nanosci 6(3):281–293

60. Chalangar E et al (2018) Influence of morphology on electrical and optical properties of graphene/Al-doped ZnO-nanorod composites. Nanotechnology 29(41):415201

61. Lin OH, Akil HM, Mahmud S (2009) Effect of particle morphology on the properties of polypropylene/nanometric zinc oxide (pp/nanozno) composites. Adv Compos Lett 18(3):096369350901800302

62. Hemalatha K et al (2014) Synthesis, characterization and optical properties of hybrid PVA–ZnO nanocomposite: a composition dependent study. Mater Res Bull 51:438–446

63. Shetty BG et al (2019) Effect of nano fillers on electrical, mechanical, fluorescent and third order non linear optical properties of PVA. Mater Res Express 6(7):075055

64. Dash S et al (2019) Enhanced dielectric properties and theoretical modeling of PVDF–ceramic composites. J Mater Sci: Mater Electron 30(21):19309–19318

65. Rithin Kumar NB, Crasta V, Praveen BM, Kumar M (2015) Studies on structural, optical and mechanical properties of MWCNTs and ZnO nanoparticles doped PVA nanocomposites. Nanotechnol Rev 4(5):457–467

66. Gao Y et al (2006) Consecutive solvent evaporation and co-rolling techniques for polymer multi-layer hollow fiber preform fabrication. J Mater Res 21(9):2246–2254

67. Duan C-G et al (2003) Theoretical study on the optical properties of polyvinylidene fluoride crystal. J Phys: Condens Matter 15(22):3805

68. Cheng H-P et al (2014) Electronic structures and optical properties of poly (vinylidene fluoride) crystals. Acta Phys-Chim Sinica 30(2):281–288

69. El Hamidi A et al (2018) Refractive index controlled by film morphology and free carrier density in undoped ZnO through sol-pH variation. Optik 158:1139–1146

70. Ben-David M, Engel L, Shacham-Diamand Y (2017) Spectroscopic ellipsometry study of spin coated P (VDF-TrFE-CTFE) thin films and P (VDF-TrFE-CTFE)/PMMA blends. Microelectron Eng 171:37–43
71. Tsoulos T et al (2017) A closer look at the physical and optical properties of gold nanostars: an experimental and computational study. Nanoscale 9(11):3766–3773
72. Livi A, Levita G, Rolla P (1993) Dielectric behavior at microwave frequencies of an epoxy resin during crosslinking. J Appl Polym Sci 50(9):1583–1590

Authors and Affiliations

M. Yousaf[1] · M. Junaid Iqbal Khan[1] · Zarfishan Kanwal[1] · Shahid M. Ramay[2] · Hamid Shaikh[3] · Murtaza Saleem[4]

✉ Murtaza Saleem
  murtaza.saleem@lums.edu.pk

1 Laboratory of Theoretical and Experimental Physics, Department of Physics, Bahauddin Zakariya University, Multan 60800, Pakistan

2 Physics and Astronomy Department, College of Science, King Saud University, Riyadh 11451, Saudi Arabia

3 Chemical Engineering Department, SABIC Polymer Research Center (SPRC), King Saud University, P.O. Box 800, Riyadh 11421, Saudi Arabia

4 Department of Physics, SBASSE, Lahore University of Management Sciences, Lahore 54792, Pakistan